Acta Biomaterialia 95 (2019) 337–347

Contents lists available at ScienceDirect

Acta Biomaterialia

journal homepage: www.elsevier.com/locate/actabiomat

Full length article

Nanotopographical regulation of pancreatic islet-like cluster formation from human pluripotent stem cells using a gradient-pattern chip ☆

Jong Hyun Kim [a,c,d], Bo Gi Park [b], Suel-Kee Kim [e], Dong-Hyun Lee [b], Gyung Gyu Lee [a], Deok-Ho Kim [f,g], Byung-Ok Choi [c,d,h,*], Kyu Back Lee [b,*], Jong-Hoon Kim [a,*]

[a] Laboratory of Stem Cells and Tissue Regeneration, Department of Biotechnology, College of Life Sciences and Biotechnology, Korea University, Seoul 02841, Republic of Korea
[b] School of Biomedical Engineering, College of Health Science Korea University, Seoul 02841, Republic of Korea
[c] Stem Cell and Regenerative Medicine Institute, Samsung Medical Center, Seoul 06351, Republic of Korea
[d] Department of Medicine, Sungkyunkwan University School of Medicine, Gyeonggi, Republic of Korea
[e] Department of Legal Medicine, Korea University College of Medicine, Seoul 02841, Republic of Korea
[f] Department of Bioengineering, University of Washington, Seattle, WA 98195, USA
[g] Institute for Stem Cell and Regenerative Medicine, University of Washington, Seattle, WA 98109, USA
[h] Department of Neurology, Samsung Medical Center, Sungkyunkwan University School of Medicine, Seoul, Republic of Korea

ARTICLE INFO

Article history:
Received 14 August 2018
Received in revised form 3 December 2018
Accepted 5 December 2018
Available online 6 December 2018

Keywords:
Human pluripotent stem cells
Nanopillar
Nanopore
Topographical cues
Pancreatic endocrine cells

ABSTRACT

Bioengineering approaches to regulate stem cell fates aim to recapitulate the *in vivo* microenvironment. In recent years, manipulating the micro- and nano-scale topography of the stem cell niche has gained considerable interest for the purposes of controlling extrinsic mechanical cues to regulate stem cell fate and behavior *in vitro*. Here, we established an optimal nanotopographical system to improve 3-dimensional (3D) differentiation of pancreatic cells from human pluripotent stem cells (hPSCs) by testing gradient-pattern chips of nano-scale polystyrene surface structures with varying sizes and shapes. The optimal conditions for 3D differentiation of pancreatic cells were identified by assessing the expression of developmental regulators that are required for pancreatic islet development and maturation. Our results showed that the gradient chip of pore-part 2 (Po-2, 200–300 nm diameter) pattern was the most efficient setting to generate clusters of pancreatic endocrine progenitors (PDX1+ and NGN3+) compared to those of other pore diameters (Po-1, 100–200 or Po-3, 300–400 nm) tested across a range of pillar patterns and flat surfaces. Furthermore, the Po-2 gradient pattern-derived clusters generated islet-like 3D spheroids and tested positive for the zinc-chelating dye dithizone. The spheroids consisted of more than 30% CD200 + endocrine cells and also expressed NKX6.1 and NKX2.2. In addition, pancreatic β- cells expressing insulin and polyhormonal cells expressing both insulin and glucagon were obtained at the final stage of pancreatic differentiation. In conclusion, our data suggest that an optimal topographical structure for differentiation to specific cell types from hPSCs can be tested efficiently by using gradient-pattern chips designed with varying sizes and surfaces.

Statement of Significance

Our study provides demonstrates of using gradient nanopatterned chips for differentiation of pancreatic islet-like clusters.

Gradient nanopatterned chips are consisted of two different shapes (nanopillar and nanopore) in three different ranges of nano sizes (100–200, 200–300, 300–400 nm). We found that optimal nanostructures for differentiation of pancreatic islet-like clusters were 200–300 nm nano pores.

Cell transplantation is one of the major therapeutic option for type 1 diabetes mellitus (DM) using stem cell-derived β-like cells. We generated 50 um pancreatic islet-like clusters in size, which would be an optimal size for cell transplantation. Futuremore, the small clusters provide a powerful source for cell therapy.

☆ Part of the Cell and Tissue Biofabrication Special Issue, edited by Professors Guohao Dai and Kaiming Ye.

* Corresponding authors at: Building 1/Room 304, West Building, College of Life Sciences and Biotechnology, Science Campus, Korea University, 145 Anam-ro, Sungbuk-gu, Seoul 20841, Republic of Korea (J.-H. Kim). Hana Science Hall B room 469, School of Biomedical Engineering, College of Health Science Korea University, 145 Anam-ro, Seoungbuk-gu, Seoul 02841, Republic of Korea (K.B. Lee). Department of Neurology, Samsung Medical Center, Sungkyunkwan University School of Medicine, 81 Irwon-ro, Gangnam-gu, Seoul 06351, Republic of Korea (B.-O. Choi).

E-mail addresses: bochoi77@hanmail.net (B.-O. Choi), kblee@korea.ac.kr (K.B. Lee), jhkim@korea.ac.kr (J.-H. Kim).

https://doi.org/10.1016/j.actbio.2018.12.011

Our findings suggest gradient nanopatterned chip provides a powerful tool to generate specific functional cell types of a high purity for potential uses in cell therapy development.

1. Introduction

The topographical environment of tissues contributes to the regulation of cell fate and behavior [1]. During human organogenesis, developing structures are not only exposed to biochemical soluble factors, but also receive various topographical cues from micro- and nano-scale surface structures in the surrounding microenvironment. These topographical factors occur in different shapes and sizes, thereby providing a highly dynamic environment [2–4]. The tissue microenvironment consists of various micro- and nano-scale extracellular matrix (ECM) components such as collagen, fibronectin, and laminin [5,6]. However, current *in vitro* culture systems have largely relied on 2-dimensional (2D) flat surfaces with a physiologically relevant ECM coating to culture a range of cell types, including somatic cells, cancer cells, and stem cells. To more closely mimic the *in vivo* microenvironment, recent studies have applied surface nanopatterning in combination with biochemical factors and demonstrated that topographical features regulate cellular functions, including self-renewal, proliferation, and differentiation of various types of human pluripotent stem cells (hPSCs) [7,8]. Moreover, these biomimetic topographical materials may serve as important mediators for facilitating adhesion localization, integrin clustering, cytoskeletal reorganization, and mechanotransduction [9].

Topographical studies investigating stem cell behavior have focused on identifying optimal conditions of shape and size using various forms of micro- and nano-scale structures (fibers, ridges, and pores) made of materials such as polystyrene [PS], polydimethylsiloxane, titanium (II) oxide, silicon dioxide, and nickel, to regulate differentiation of human embryonic stem cells (hESCs) and human mesenchymal stem cells [10–13]. Adipose tissue-derived stem cells have previously been shown to differentiate into adipocytes and osteocytes when cultured on 200- nm nanopore- and nanopillar-patterned chips fabricated with PS substrates [14]. In addition, a recent study using a nanopillar gradient pattern demonstrated that hPSCs had a propensity to remain undifferentiated in the 120–170 nm range compared with other ranges tested (170–290 nm and 290–360 nm) [7].

Stem cell-based approaches for cell therapy and *in vitro* drug screening require high efficiency in production of particular cell types from patient-derived hPSCs. We and others have demonstrated successful differentiation of functional pancreatic β-cells, dopaminergic neurons, and hepatocytes from hPSCs [15–18]. However, the differentiation efficiency and function of hPSC-derived pancreatic β-cells is still relatively low compared to other cell types both in 2D and 3D conditions using conventional culture systems [19–21]. By applying nanotopographical control using a single sized-nanopatterned chip, we previously showed that pancreatic differentiation from hPSCs was significantly enhanced when induced on a PS substrate with an array of 200 nm pores compared with a flat surface or other pore diameters (130, 170, and 230 nm) in 2D differentiation conditions [12]. As many studies have shown efficiency in generating functional pancreatic cells can be enhanced in 3D conditions compared to 2D conditions [22], therefore adapting nanotopographical control into 3D structure formation is desirable. In addition, single sized-nanopatterns have limited utility for testing wide ranges of topographical cues compared to a gradient nanopattern that is designed for a diverse range of patterns on a single chip.

In this study, we developed gradient nanopatterned chips to improve the efficiency of screening wide ranges of topographical cues and tested them for 3D differentiation of pancreatic β-cells from hPSCs. Our results show that the Po-2 pattern (200–300 nm diameter) strongly promotes formation of pancreatic islet-like clusters.

2. Experimental section

2.1. Fabrication of gradient nanopatterned substrate

Ultrapure aluminum plates (99.999%, Goodfellow, UK) were polished electrochemically (perchloric acid; absolute ethanol = 1:4) at 20 V and 7 °C. Two types of anodic aluminum oxide molds were fabricated: oxalic AAO (O-AAO) and phosphoric AAO (P- AAO). Polished aluminum plates were first anodized in oxalic acid (0.1 M) and phosphoric acid (deionized water:methanol:phosphoric acid = 59:40:1) at 40 V and 193 V for 12 h, then etched with chromic acid solution (9 g, 193 V for 12 h, and 20.3 mL phosphoric acid in 500 mL deionized water). The well-ordered porous AAOs were anodized again under the same conditions for 3 min and 4 h, and modulated with a gradually increasing dipping time in phosphoric acid solution using a tensiometer. A self-assembled heptadecafluor0-1,1,2,2-tetrahydrodecyl- trichlorosilane (HDFS) monolayer was coated onto the modulated gradient AAO molds. The surface of each AAO was first hydroxylated with piranha solution (35% H2SO4:H2O2 = 7:3, v/v). The HDFS monolayer was then assembled on the surface using a 3 mM water-free HDFS solution of n-hexane. PS samples (polystyrene) with gradient pillar nanopatterns were fabricated by thermal nanoimprinting with AAO molds containing a gradient of nanometer-scale pores using a nanoimprinting device, NANOSISTM610 (Nano & Device, South Korea). PS polymer sheets (1.2 mm thickness, Goodfellow, UK) of 700 mm^2 (35 mm × 20 mm) were heated at 130 °C for 10 min and pressed at 3 bar for 100 s. PS sheets were detached from the AAO molds at room temperature. A sectioned gradient nanopattern was fabricated by modulating the pores of second anodized AAOs with a gradually increasing dipping time in phosphoric acid solution using a tensiometer. PS samples with gradient pore nanopatterns were fabricated by thermal nanoimprint with pillar containing PMMA (polymethylmethacrylate) molds by heating PS sheet at 135 °C for 10 min and pressed at 2 bar for 90 sec. The PMMA mold with gradient pillar nanopatterns were fabricated by nanoimprinting with AAO molds containing gradient pores by heating PMMA sheet (1.1 mm thickness, Goodfellow, UK) at 190 °C for 10 min and pressed at 3 bar for 100 s. The chemical characteristics of the surfaces of PS nanopatterns are the same as that of the flat PS sheet, because PS polymer sheets are simply nanoimprinted with the AAO and PMMA molds.

In order to determine the optimal shape and size of nanopattern chip for efficient pancreatic cluster formation from hPSCs, six different gradient nanopattern chips with three different ranges of sizes (between 100–400 nm) for two shapes (pillar or pore) were tested. The different ranges of sizes for each gradient chips were as follows: pillar (Pi-1, 100–190 nm; Pi-2, 190–270 nm; Pi-3, 270–360 nm) and pore (Po-1, 100–200 nm; Po-2, 200–300 nm; Po-3, 300–400 nm). All the features in the nanopattern possess 450 nm pitch (center-to-center distance). The diameters of pores

became larger in comparison with those of pillars during the two-step thermal nanoimprinting using AAO and PMMA mold.

2.2. hPSC culture

Unless otherwise noted, all cell culture media and reagents were obtained from Thermo-Fisher Scientific (Waltham, MA, USA). H1 hESCs (WiCell Research Institute, Madison, WI, USA, passages 30–40) were maintained on mitomycin C- treated (10 μg/mL, Roche, Mannheim, Germany) mouse embryonic fibroblast feeder cells in a mixture of Dulbecco's Modified Eagle Medium and Ham's F-12 (DMEM/F12, 1:1) supplemented with 20% KnockOut serum replacement, 1 mM nonessential amino acids, 0.1 mM β-mercaptoethanol (Sigma-Aldrich, St Louis, MO, USA), 100 U/mL penicillin G, 100 μg/mL streptomycin, and 10 ng/mL human FGF2 (R&D Systems, Minneapolis, MN, USA). Every 5–6 days, hESCs colonies were subcultured by treating with 1 mg/mL collagenase type IV. For feeder-free culture, the undifferentiated hESCs colonies expanding on feeder cells were dissociated into single cells with TrypLE Select, plated at a concentration of 8×10^4 cell/cm^2 on a Matrigel-coated culture plates (BD Biosciences, San Jose, CA, USA), and cultured in mTeSR™1 medium. Cells were plated in medium containing 10 μM Y27632, a ROCK inhibitor (Sigma-Aldrich), to increase cell survival upon dissociation. The ROCK inhibitor was removed from the medium 24 h after plating and cells were passaged twice before inducing differentiation. All cell culture studies were performed in a standard humidified atmosphere of 5% CO2 and 21% O2 at 37 °C.

2.3. Differentiation into pancreatic islet-like cells using gradient nano pattern chips

A schematic diagram illustrating the overall strategy to generate pancreatic islet-like cells on a gradient nano pattern chip is presented in Fig. 2. The detailed protocol is described below.

Stage I: Undifferentiated hESCs. Single-cell suspensions of hESCs were seeded at 2×10^5 cells/cm^2 on Matrigel-coated culture dishes, without a feeder layer, in mTeSR1 medium supplemented with the 10 μM Y27632. Twenty-four hours after replating, the ROCK inhibitor was removed from the medium and cells were cultured for 1 day.

Stage II: Definitive endodermal cells. hESCs were differentiated into mesendodermal cell by treating with 100 ng/mL Activin A (R&D Systems) and 25 ng/mL Wnt3a (R&D Systems) for one day and further differentiated into definitive endodermal cell in the presence of Activin A with 0.2% fetal bovine serum (FBS) for 2 days.

Stage III: Pancreatic progenitors. Differentiated cells were dissociated by treatment with TrypLE select (Invitrogen) for 5 min and the 1×10^6 cells were seeded on each gradient chip. The six gradient chips and flat surface culture dishes were pretreated with 10 μg/mL fibronectin (Roche, Mannheim, Germany) for overnight at 4 °C prior to use. Single dissociated definitive endodermal cells (stage II) were cultured for 6 days in DMEM supplemented with B27, 2 μM retinoic acid (RA), 50 ng/mL Noggin, and 30 ng/mL FGF7 (R&D Systems).

Stage IV: Pancreatic endocrine progenitors. Pancreatic progenitors (stage III) were cultured for 6 days in DMEM containing 1 ng/mL FGF2, 50 ng/mL Activin βB (R&D Systems), 30 ng/mL vascular endothelial growth factor (VEGF) (R&D Systems), and 100 μM ascorbic acid (Sigma- Aldrich). Cell aggregates, which were ≥ 100 um in diameter and positive for both PDX1 and NGN3 were consider hPSC-derived islet-like clusters. The average number of islet-like cluster per a microscopic filed was obtained under 10X magnification.

Stage V: Pancreatic endocrine cells. Cell clusters at the end of stage IV were treated with collagenase IV (200 units/ml, Invitrogen) at 37 °C for 10 min and detached individual cells and clusters were separated by consecutive passaging through sterile 50 and 70 um nylon cell strainers. The harvested cell clusters were cultured in CMRL-1066 medium containing B27 and Exendin 4 (50 ng/ml, Sigma-Aldrich) for 12 days.

2.4. Real-time quantitative PCR (qRT-PCR)

Differentiated cells were analyzed by qRT-PCR using the iQTM SYBR® Green Supermix (Bio- Rad, Hercules, CA, USA) system. Primer sequences (Applied COSMO Genetech, Seoul, Korea) are listed in Table 1. Briefly, 20 μl of the qRT-PCR mixture contained 10 μl 2 × iQTM SYBR® Green Supermix, 50 ng cDNA, and 1 μl of the 20 × SYBR® Green expression assays. The threshold cycle (CT) of target genes was analyzed with the CFX-96 real-time PCR system (Bio-Rad). The comparative CT method (2-ΔΔCt) was used to determine the relative expression levels of target genes, normalized to *GAPDH*.

2.5. Western blotting analysis

Cells were harvested in RIPA lysis buffer (Upstate, Charlottesville, VA, USA) supplemented with a protease inhibitor cocktail tablet (Roche). Equal amounts of protein (50 μg/lane) were separated by electrophoresis on NuPageTM 4–12% Bis-Tris polyacrylamide gels and transferred to PVDF membranes. Membranes were incubated with primary antibodies against PDX1 (1:200; AF2419, R&D Systems) and β-actin (1:200, sc-1615, Santa Cruz Biotechnology) overnight at 4 °C. The membranes were then rinsed with 1 × Tris-buffered saline supplemented with 0.05% Tween 20 and incubated with the appropriate horseradish peroxidase-conjugated secondary antibodies (1:10,000; sc-2020, Santa Cruz Biotechnology) for 1.5 h at room temperature. Immunoreactive proteins were detected using ECL Plus reagents (GE Healthcare, Chalfont St. Giles, UK).

2.6. Immunofluorescence staining

Cells were fixed in 4% paraformaldehyde in phosphate-buffered saline (PBS). After permeabilization in 0.3% Triton X-100 in PBS and blocking in 10% donkey serum with 0.1% bovine serum albumin (BSA) in PBS, sections were incubated with primary antibodies at 4 °C overnight. Isotype mouse IgG or normal donkey serum (Sigma-Aldrich) were used as negative controls. The primary antibodies were human Oct4 (1:400 sc-5279, Santa Cruz Biotechnology), Nanog (1:200, AF1997, R&D Systems), SSEA4 (1:200, MAB4304, Millipore Billerica), Sox17 (1:400, AF1924, R&D Systems), PDX1 (1:200, AF2419, R&D Systems), Neurogenin3 (1:300 sc-136002, Santa Cruz Biotechnology), Islet1 (1:200, AF1837, R&D Systems), insulin (1:500, 4011-0F, Linco, St Charles, MO), and glucagon (1:500, G2654, Sigma-Aldrich). Samples were then washed with PBS and probed with appropriate fluorescence-tagged secondary antibodies (1:400; A21207, A21230, A11016, A21202, and A11055, Invitrogen) in 0.1% BSA/PBS at room temperature. An Apotome-Axiovert 200M fluorescence microscope (Carl Zeiss, Jena, Germany) and confocal laser scanning microscope (Carl Zeiss) were used to visualize cells after counterstaining of nuclei with 4′,6-diamidino-2-phenylindole (DAPI; 1:1000; 100-43-6, Sigma-Aldrich).

2.7. Flow cytometry

hESC-derived pancreatic cells were assessed by flow cytometry to evaluate the efficiency of differentiation. Surface marker staining was accomplished by washing the cells with PBS supplemented with 1% FBS, followed by incubation for 30 min at 4 °C with

Table 1
Primers and reaction conditions for qPCR.

Gene	Forward (5′→3′)	Reverse (5′→3′)	Product size (bp)	Annealing temperature, cycle number
SOX17	cgcacggaatttgaacagta	ggatcagggacctgtcacac	181	60 °C, 30
CXCR4	cactacttcagaatttcctg	gcccatttcctcggtgtagtt	80	60 °C, 30
FOXA2	ttctccatcaacaacctcatgtcc	gtagtgcatcacctgttcgtagg	107	57 °C, 30
MNX1	gcaccagttcaagctcaac	gctgcgtttccatttcatcc	127	58 °C, 30
PDX1	accaaagctcacgcgtggaaa	tgatgtgtctctcggtcaagtt	200	64 °C, 35
NKX6.1	ggcctgtacccctcatcaag	ccggaaaaagtgggtctcgt	78	57 °C, 30
NEUROD 1	tacatctgggctctgtcgga	ccttgcaaagcgtctgaac	79	60 °C, 30
GAPDH	agccacatcgctcagacac	gcccaatacgaccaaatcc	60	58 °C, 35

anti-CXCR4 (BD Biosciences) and anti-CD200 (BD Biosciences). Data were acquired using a BD-FACS Calibur (BD, San Jose, CA, USA). Three independent biological experiments were performed for each marker. Data were analyzed with CellQuest software (version 7.2, BD).

2.8. Dithizone (DTZ) staining

The cells were incubated with 10 μg/mL DTZ (Merck, Whitehouse Station, NJ, USA) at 37 °C for 15 min. After the dishes were rinsed three times with Hank's Balanced Salt Solution, clusters stained crimson red were examined under a stereomicroscope.

2.9. Statistical analysis

Data represent means ± standard deviation of at least three independent experiments performed in triplicate. Group means were analyzed using a Student's *t*-test for pairwise comparisons. For multiple comparisons, one-way ANOVA followed by a Tukey's test and GraphPad PRISM 5 was used. Significant differences were reported when the p value was less than 0.05.

3. Results

3.1. Fabrication of the pillar/pore type polystyrene (PS) G-NP substrate

Three sections of AAO molds with regular arrays of pores were fabricated via two-step anodization in phosphoric acid. AAOs with nanometer-scale pore gradients were achieved by slowly increasing the dipping time in phosphoric acid solution at 30 °C to widen the pores. The pore diameter of the three sections of AAO molds increased linearly as a function of dipping time (Fig. 1A, B). The isotropic etching ratio was 0.65 nm/min, which was similar to previously reported values. Patterning of the pillar/pore type G-NP was achieved by thermal nanoimprinting of three-sectioned AAO molds with a nanopore gradient. PS was selected as the base material because it is the most commonly used material for cell culture dishes. A pillar type PS G-NP was achieved via one-step thermal nanoimprinting of three- sectioned AAO molds (Fig. 1B). In the first nanoimprinting, a PS nanopillar array was constructed using three-sectioned gradient AAO molds. A pore type PS gradient surface was also achieved via two-step thermal nanoimprinting of three-sectioned AAO molds (Fig. 1C). In the first nanoimprinting, a poly (methyl methacrylate) (PMMA) nanopillar array was constructed using three-sectioned gradient AAO molds on a PMMA sheet. The second nanoimprinting was carried out by thermal nanoimprinting using the PMMA nanopillar array to PS sheet. The diameter of the pillar type G-NP was confirmed by measuring average diameters in scanning electron microscopy (SEM) images (Fig. 1D). The diameters of the three-sectioned pore type G-NP were also well-matched to diameters of pillar type G-NP (Fig. 1e). These results demonstrate that pillar/pore type G-NP can be successfully constructed by using thermal nanoimprinting for optimization of cell responses to nanostructured substrates. Neither the control nor the measurement of the height of pillars and the depth of pores was performed. This is because the height of pillars and the depth of the pores appears to be not important unless cell membrane sinks deeply inside the nanometer scale features. In our observation, the cell membrane did not sink deeply between the pillars or inside the pores when we did experiments in the range of lateral dimension in this study due to the tension of the cell membrane (data not shown).

3.2. Endodermal induction and pancreatic cell differentiation

Pancreatic cell differentiation was performed using the following four differentiation steps: induction of definitive endodermal cells (stage II), pancreatic progenitors (stage III), pancreatic endocrine progenitors (stage IV), and pancreatic endocrine cells (stage V). The differentiation medium was supplemented with multiple combinations of biosoluble factors, including Wnt3a, Activin A, RA, Noggin, FGF2, Activin βB, VEGF, and Exendin-4 at respective stages (Fig. 2A). Stage I conditions involved the maintenance of hESCs in feeder-free conditions. Cells were plated and cultured for 3 days in mTeSR1 medium, which supports the formation of compact undifferentiated colonies. Under this culture condition, hESCs expressed a high level of key pluripotency regulators such as OCT4, NANOG, and SSEA4 (Fig. S1A). Activation of Activin and Wnt signaling was previously shown to induce specification of anterior definitive endoderm from hPSCs by upregulating expression of *SOX17*, *FOXA2*, and *CXCR4* [23,24]. For stage II, differentiation to definitive endodermal cells was induced by treatment with Wnt3A and Activin A on Matrigel-coated conventional flat-bottom dishes for 3 days. Immunocytochemical analyses revealed significantly increased expression of SOX17 in almost all the cells on day 3 without detectable PDX1 expression, demonstrating that cells were differentiated to definitive endoderm in a highly controlled manner (Fig. S1B). qRT-PCR analysis showed that the expression of *SOX17*, *FOXA2*, and *CXCR4* in differentiated cells was at least 20-fold greater than in undifferentiated hESCs (Fig. S1C). Additionally, flow cytometric analyses revealed that 88.75% of differentiated cells expressed CXCR4 (Fig. S1D). These results demonstrate that treatment with Activin A and Wnt3a for 3 days produces a high percentage of definitive endodermal cells without any purification steps. These populations were then used to generate pancreatic endodermal cells.

3.3. Optimal nanopattern conditions for pancreatic endocrine cluster formation

We next investigated the nanotopographical conditions that regulate differentiation of definitive

endodermal cells into pancreatic cells (stage III) by testing three different chips of gradient nanopillar patterns (Pi-1,2,3) and three different chips of gradient nanopore patterns (Po-1,2,3), as well as conventional flat surface dishes coated with fibronectin

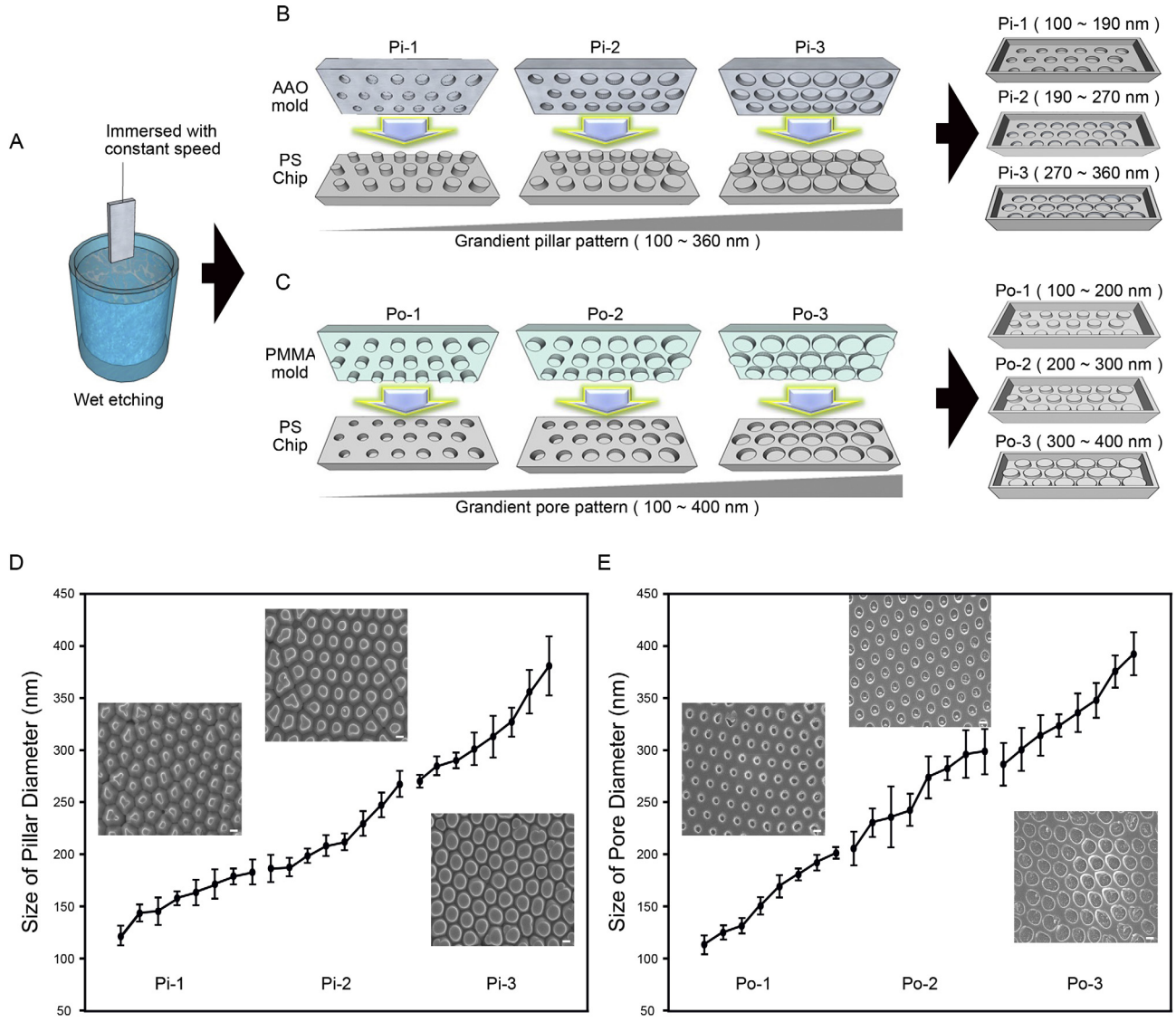

Fig. 1. Characterization of pillar- and pore-type gradient nanopatterns**.** (A) Schematic illustration of wet etching process for making phosphoric gradient AAO mold. (B, C) Schematic illustration of the thermal nanoimprinting process for the generation of pillar (pi)- and pore (po)-type PS nanopatterns. (D, E) Graph illustrating the size variation of pillar and pore types of three-sectioned phosphoric gradient nanopatterns. . Scale bars, 200 nm (all panels in D and E).

(Fig. 2A). There was no difference of fibronectin adsorption among the nanopatterns when observing the surfaces with SEM (data now shown). The definitive endoderm cells differentiated in stage II were dissociated and attached to the substrates to determine the induction efficiency of pancreatic bud-like formation. The pancreatic bud in early embryos consists of foregut endoderm cells (PDX1+), which gradually develop into pancreatic progenitors and endocrine progenitors [25,26]. Nuclear staining (DAPI) showed that the dissociated definitive endoderm cells adhered successfully under all conditions 24 h after plating (Fig. 2B). No significant differences were found in the number of cells that adhered to different nanopatterned surfaces (Fig. 2C).

Our protocol for pancreatic differentiation was established based on *in vivo* embryonic development, including the formation of dorsal foregut endoderm to dorsal pancreatic bud and islets [27]. We further investigated the effect of nanotopography in conjunction with treatment with the developmental signaling factors RA and Noggin for 6 days (stage III). Morphological analysis at the end of stage III showed that the gradient Po-2 pattern significantly induced the formation of out-growing bud-like structures, compared with other types and the flat surface dish. The bud-like structures displayed thin and linear margins between cell aggregates (Fig. S2A, red dashed box). Many of the pancreatic bud-like clusters that differentiated on the gradient Po-2 pattern chip expressed high levels of PDX1. Expression of a pancreatic progenitor marker NKX6.1 was also detected in a subset of the PDX1-expressing population (Fig. S2B).

Pancreatic β-cells develop sequentially from definitive endoderm cells to pancreatic progenitors, endocrine progenitors, and endocrine cells. We next induced pancreatic endocrine cluster formation by supplementing the culture medium with FGF2, Activin βB, and VEGF for 6 days (stage IV). The gradient Po-2 pattern profoundly enhanced 3D cluster formation, as determined by counting the number of cell clusters in the seven different patterns (Fig. 2D, E). PDX1 and NGN3 play important roles in the differentiation of pancreatic progenitors into endocrine progenitors [28]. Multipotent NGN3-expressing cells differentiate into unipotent islet precursors and pancreatic hormone cells [29]. Co-expression of

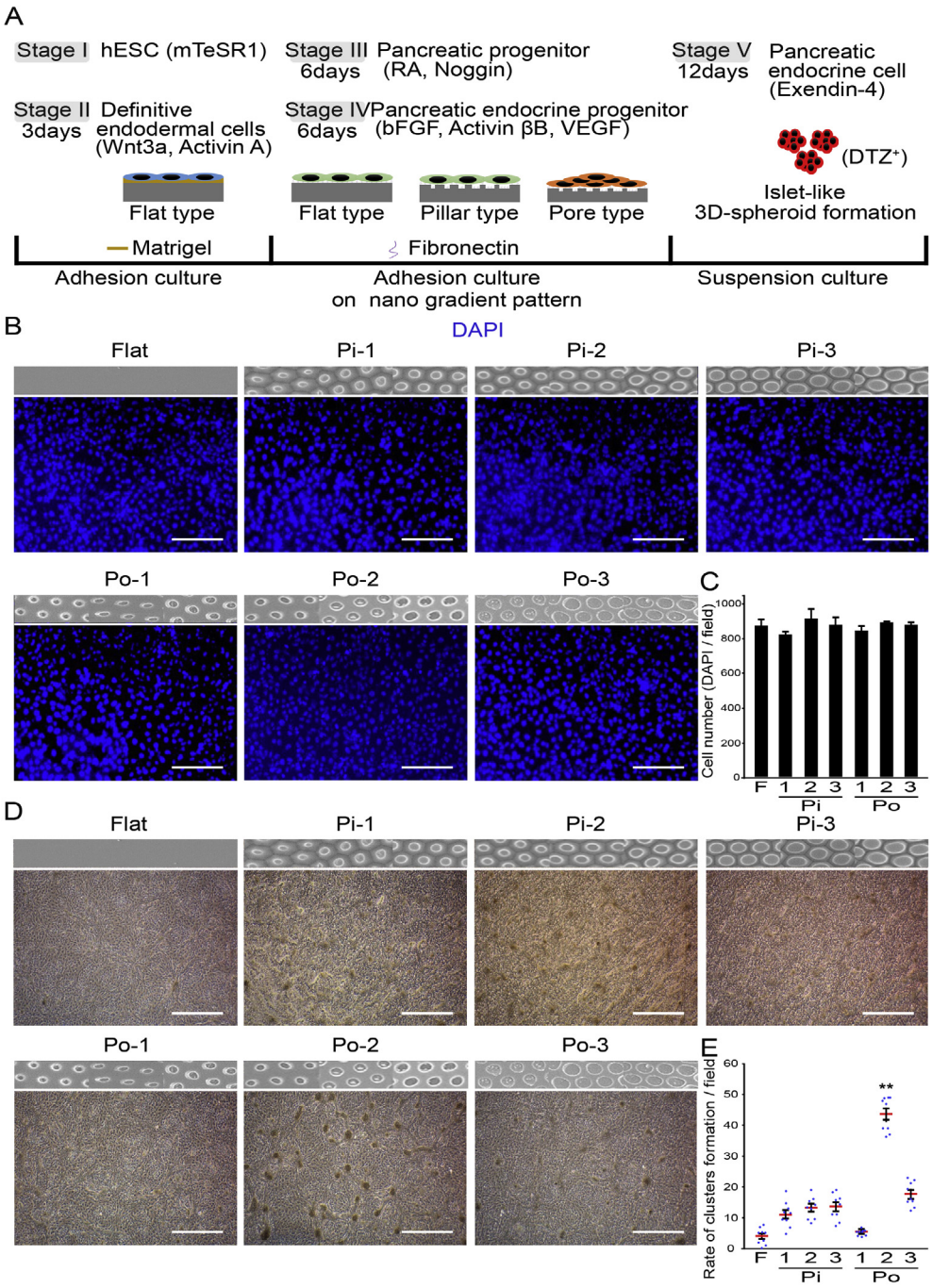

Fig. 2. Generation of pancreatic islet-like clusters on different gradient nanopatterns. (A) Schematic representation of culture conditions at each stage of differentiation illustrating the morphological changes from stage I (hESCs) to V (3D islet-like spheroids). Definitive endodermal cells (Stage II) obtained from differentiation of hESCs were cultured on flat or different gradient nanopatterns in Stages III and IV. (B and C) Quantification of attached cells on the six different gradient patterns or the flat surface at the end of stage II. Cells were stained with DAPI (blue) in (B) and quantified in (C). (D) Phase-contrast images of cells at stage IV illustrating the pancreatic endocrine cluster-like formation on seven different surfaces following treatment with FGF2, Activin βB, and VEGF. (E) Quantitative analysis of endocrine cluster-like formation on six gradient-pattern chips and one flat surface. $^{*}p < 0.05$, $^{**}p < 0.01$ vs. flat surface. Scale bars, 150 μm (all panels in B and D). (For interpretation of the references to colour in this figure legend, the reader is referred to the web version of this article.)

PDX1 and NGN3 protein was significantly higher in the differentiated 3D clusters on the Po-2 pattern compared with the other nanopattern chips (Fig. 3A, C). The gradient Po-2 pattern chip induced significantly higher mRNA expression of the pancreatic progenitor genes *PDX1* and *NKX6-1*, as well as endocrine islet progenitor genes *MNX1* and *NEUROD1* relative to the other nanopattern chips (Fig. 3D). Importantly, the highest level of PDX1 protein expression was observed in cells grown on the gradient Po-2 pattern at stage IV (Fig. 3E). These data show that the gradient Po-2 pattern most efficiently induced PDX1 and NGN3 expression in endocrine clusters compared with the other gradient patterns and indicate that pancreatic bud-like cluster formation was successfully induced from definitive endoderm cells by the gradient Po-2 pattern.

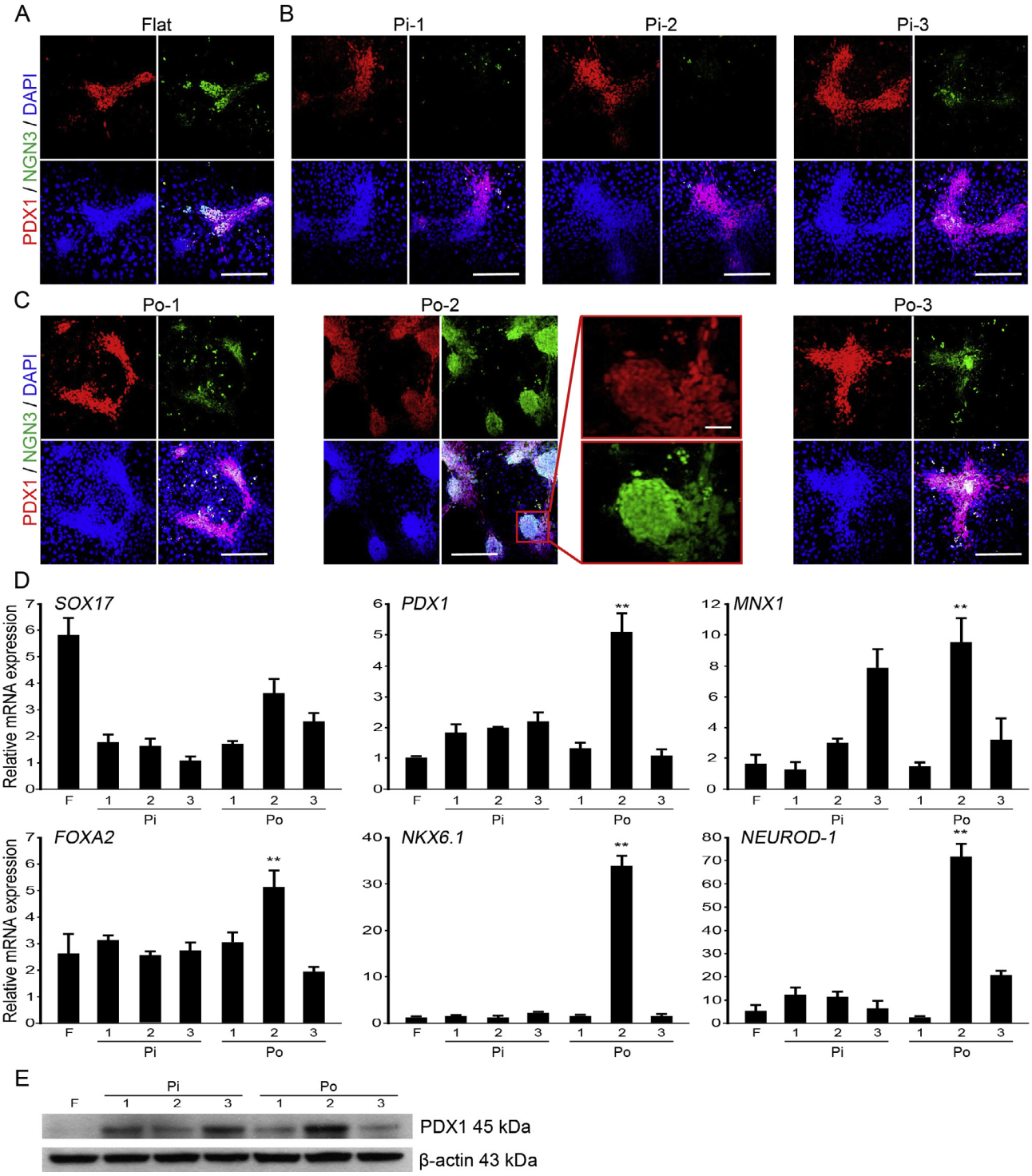

Fig. 3. Identification of pancreatic endocrine progenitors on gradient nanopattern chips. (A-C) Immunofluorescent staining of double-positive PDX1 (red) and NGN3 (green) cells, representing pancreatic progenitors differentiated on seven different surfaces in the presence of RA and Noggin at the end of stage IV. Cells were counterstained with DAPI (blue). (D) qRT- PCR showing the relative expression levels of markers of definitive endoderm (*SOX17* and *FOXA2*), pancreatic progenitors (*PDX1* and *NKX6-1*), and pancreatic endocrine progenitors (*MNX1* and *NEUROD1*). (E) Western blots showing the expression level of the pancreatic progenitor marker PDX1 in cells cultured on the indicated surfaces. $^{*}p < 0.05$, $^{**}p < 0.01$ vs. flat surface (F). Scale bars, 150 μm in all panels of A-C except for the magnification shown in the right panels of Po-2 in C representing 50 μm (For interpretation of the references to colour in this figure legend, the reader is referred to the web version of this article.)

3.4. Formation of pancreatic islet-like clusters and polyhormonal spheroids

Less than five cell clusters per a microscopic filed were seen on the flat substrate as shown in Fig. 2E and the numbers were too small to proceed for further differentiation to the pancreatic progenitors or islets as 3D spherical clusters. We thus next tested the formation of islet-like spheroids from the gradient Po-2 pattern-derived endocrine clusters (PDX1+ and NGN3+) by further differentiating them in the presence of Exendin-4 for 12 days (stage V). The average diameter of endocrine clusters grown on the gradient Po-2 pattern at the end of stage IV was

47.6 ± 10 μm, which is comparable to a human adult pancreatic islet (Fig. 4A,B). These endocrine clusters were enzymatically isolated and cultured in suspension with Exendin-4 treatment (Fig. 4C). Previously, our reports and other studies demonstrated that pancreatic endocrine cells containing zinc in insulin-containing secretory granules stain red with dithizone (DTZ), and this characteristic can be used to identify a mature islet [17,30]. Most spheroids produced from hESC-derived pancreatic endocrine

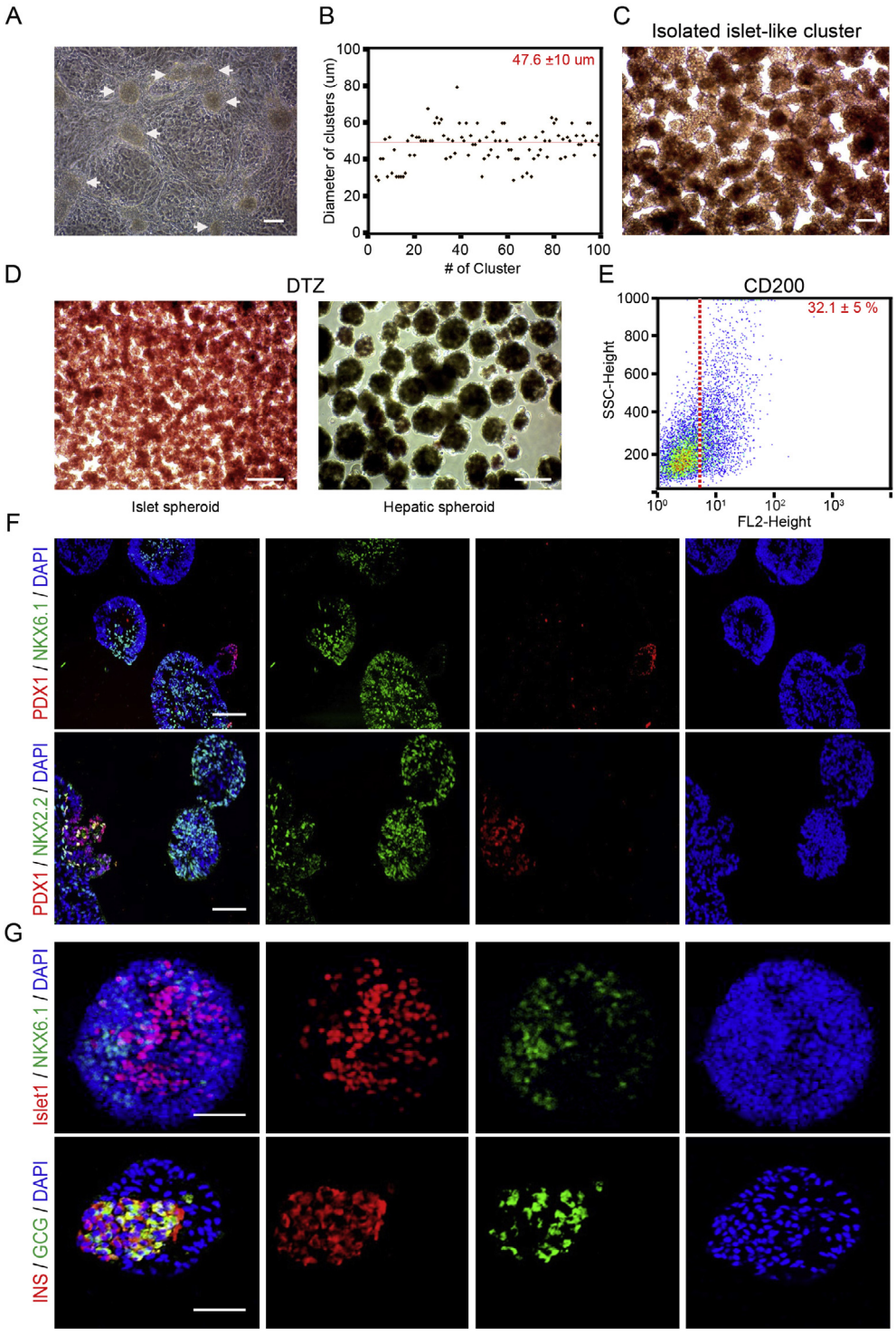

Fig. 4. Differentiation of hESC-derived pancreatic endocrine progenitors into 3D islet-like spheroids. (A) A representative phase-contrast image showing pancreatic bud-like cluster (white arrows) formation on the one-chip gradient Po-2 pattern. (B) Quantification and size distribution of pancreatic endocrine clusters produced on the Po-2 pattern chip. (C) Phase contrast Images of spheroids harvested from the Po-2 pattern chip after treatment with collagenase IV. (D) Image illustrating DTZ+ aggregates after treatment with Exendin-4 for 4 days. (E) Flow cytometry plots showing the percentage of cells expressing the pancreatic endocrine cell marker CD200 in DTZ+ spheroids. (F) Immunofluorescent staining of DTZ+ aggregates with anti-PDX1 (red), NKX6.1 (green), and NKX2.2 (green) antibodies. Cells were counterstained with DAPI (blue). (G) Immunofluorescent staining of pancreatic endocrine markers for Islet1 (red) and NKX6.1 (green) in upper panels and for insulin (INS, red) and glucagon (GCG, green) in lower panels. Cells were counterstained with DAPI (blue). Scale bars, 100 μm (A, C, and D); 200 μm (F and G). (For interpretation of the references to colour in this figure legend, the reader is referred to the web version of this article.)

progenitors stained positive for DTZ at 4 days after enzymatic isolation and Exendin-4 treatment, whereas hepatic spheroids were not stained by DTZ (Fig. 4D). The pancreatic endocrine cells express CD200 and give rise to functional insulin- producing cells [31]. Furthermore, NKX2.2 encodes a homeodomain transcription factor, which is detected in early endocrine cells, but not in pancreatic hormonal cells [32]. As expected, flow cytometric analysis revealed that a high percentage of cells (32.1% ± 5%) derived from dissociated DTZ-positive spheroids expressed CD200 (Fig. 4E). Immunocytochemical studies showed that islet-like spheroids treated with Exendin-4 for the first 4 days contained few cells positive for pancreatic progenitor marker PDX1, but a high number of cells expressing the endocrine cell markers NKX6.1 and NKX2.2 (Fig. 4F). Further induction with Exendin-4 for an additional 4 days decreased the number of NKX6.1 cells in spheroids, which contained a high number of cells expressing Islet1, a marker of pancreatic islets. These results suggest that spheroids grown on the gradient Po-2 pattern successfully differentiate into pancreatic endocrine cells, although these pancreatic islet-like spheroids still contained early polyhormonal cells that coexpressed insulin and glucagon (Fig. 4G).

4. Discussion

Nanotopographical features can serve as an *in vivo*-like microenvironment and support cell differentiation and maturation *in vitro*. In this study, we demonstrate that a gradient nanopatterned chip can identify optimal nanostructures for pancreatic differentiation from hPSCs. We tested different shapes with various sizes of nanopatterns, which were constructed in separate cell culture dishes and found that the pore shape with gradient pattern in 200–300 nm ranges were most optimal for generation of 3D pancreatic clusters from hPSCs.

Nanopatterned chips designed for each type of nanostructure in a chip may not be an efficient tool to find optimal conditions for specific cell types among various nanostructures. Our gradient pattern chips consisting of a range of different gradient diameters in a single chip providing a great advantage over single sized-patterned chips for efficiently screening multiple nanotopographical conditions. In the present study, we optimized the nanotopographical conditions for induction of pancreatic islet-like clusters by testing different types of gradient-patterned chips. The gradient nanopatterns did not influence differentiation of high-quality CXCR4 + definitive endoderm cells in the presence of Activin A, Wnt3a, and CHIR99021 (GSK-3 inhibitor), which are potent inducers of endodermal differentiation. Cells were dissociated and plated at a high density in fibronectin-coated gradient nanopatterns, which is crucial for formation of pancreatic bud structures since spheroid formation is enhanced by cell–cell interactions of definitive endoderm cells [33].

Our findings are consistent with previous studies demonstrating that the shape and density of nanostructures regulates stem cell fate [34]. A substrate featuring 200 nm pillars induced osteocyte differentiation of human mesenchymal stem cells, while 200 nm pores induced adipocyte differentiation [14]. The size of nanostructures also influences stem cell differentiation into pancreatic cells. We previously demonstrated that, during pancreatic differentiation of hESCs, cells grown on a 200 nm pore pattern showed significant upregulation of PDX1 expression compared with cells grown on pores of 130, 170, or 230 nm [12]. Our previous study also showed that 200 nm nanopore-patterned surfaces highly downregulated the expression of TAZ, which led to inhibition of pSmad 2/3 signaling and upregulation of both NGN3 and PDX1 [12]. In the present study we extended this previous observation using gradient chips by testing two different shapes, pillar and pore, and different sizes of the nanopattern for each shape. The result was comparable with our previous finding, showing that the gradient chips with sizes ranging from 200–300 nm nanopores were most useful for pancreatic differentiation. In addition, we also found that pore gradient 200–300 nm pattern was most optimal for 3D islet-like cluster formation among nanopatterns we tested. We observed that distribution of PDX1 and NGN-double positive progenitors was confined to clusters, while these cells were observed throughout the cell layer in our previous study [12]. Conventional studies of embryonic development showed that the same lineage of cells expressed common adhesion molecules, recognizing and adhering one another [34]. Thus the different spatial distribution of progenitors could be explained by a potential homotypic aggregation of cells in the dissociation and replating step of definitive endoderm at the end of stage II, which was not involved in our previous study. The exact mechanism by which 200–300 nm nanopores enhance the formation of islet-like cluster is presently unknown and remains to be elucidated. However, nanotopography affects many cellular processes, including cell adhesion, integrin clustering, and cytoskeletal reorganization [9]. Therefore it will be interesting to investigate how mechanical stimuli from nanopores regulate TAZ expression and determine the potential link between TAZ and PDX in pancreatic differentiation and islet cluster formation.

Two issues can also be discussed in relation with the enhancing mechanism of 200–300 nm nanopores for the formation of islet-like cluster. The first issue is the stiffness of the nanometer scale features inside the nanopattern. In the cases of pillar nanopatterns, the height may affect to the stiffness of pillar structures. However, in this study, meaningful results were obtained not from the pillar nanopatterns but from the pore nanopatterns. This means that the stiffness of nanometer scale features is not closely related with the biological results of this study. The second issue is the conformation of adsorbed fibronectin on the surfaces of nanopatterns. As mentioned in the experimental section, fibronectin is coated prior to the usage of nanopatterns in the stage III process for the pancreatic differentiation. We are not sure that the conformation of adsorbed fibronectin is the same among the nanopatterns. The conformation of adsorbed fibronectin may affect the results of this study. However, the conformation analysis may be another big topic, because the conformation analysis of adsorbed fibronectin on the surface of the nanopatterns is very sophisticated work. This issue may be an interesting topic for a further study.

Islet-like 3D clusters are important structures that increase functional β-cell activity [35,36]. Previously, we showed that the combination treatment of FGF2, Activin βB, and VEGF increases the number of pancreatic progenitor cells and endocrine progenitors in adherent cultures after embryoid body formation [17]. However, embryonic body formation produced PDX1-expressing clusters with a low efficiency. Pancreatic endoderm cells (FOXA2 +, PDX1+, and NGN3-) cultured on the gradient Po-2 pattern differentiated into predominantly endocrine progenitor cells (PDX1+ and NGN3+) during bud-like formation following RA treatment, and subsequently formed larger clusters after treatment with FGF2, Activin βB, and VEGF. Pancreatic buds and endocrine clusters were also found on the gradient Po-3, but at a significantly lower efficiency than those on the gradient Po-2, and were absent from the other nanopatterns. These findings suggest that the specific shape and size of nanostructures in conjunction with appropriate growth factors generate highly pure pancreatic endocrine clusters. Importantly, the result of gradient Po-2 pattern in our study confirms the previous report of the 200 nm pore pattern, which showed enhanced differentiation into pancreatic differentiation from hESCs [12]. In the present study, production rates of clusters were quite low in other substrates except the gradient Po-2 pattern. Moreover, after enzymatic treatments and consecutive

passaging through strainers, the number of clusters harvested in other substrates was not enough for the next final step of differentiation into clusters consisting of terminal endocrine cells. However, clusters generated on the gradient Po-2 pattern showed successful differentiation into pancreatic islet-like clusters, resulting in a highly pure population of small human islet-like spheroids (~50 μm).

The different diameters of pillar nanopatterns may provide not only the different cell attachment areas but also the different stiffness of matrix. But, in our study, pillar nanopatterns showed no significant results. Only the pore gradient 200–300 nm pattern showed the formation of islet-like 3D clusters. This implies that the results are related with not the stiffness of matrix but the surface topology. Further studies using a pore nanopattern possessing a gradient of narrower range or possessing an optimal specific pore diameter will be required in the near future.

The diameter of the islet spheroids was comparable to human islet spheroids (50 ± 29 μm), which is considerably smaller compared with other species, such as rabbit (64 ± 28 μm) and mouse (116 ± 880 μm) [37]. Small islet clusters (<150 μm) are reported to secrete a high level of insulin per cell compared with large islet clusters (>150 μm), and do not require large nutrient and oxygen uptake for survival [38]. In addition, these clusters stained positive for DTZ, widely used to detect human insulin-producing pancreatic islets, suggesting that the small spheroids generated in this study may be appropriate for transplantation to treat type 1 diabetes. Although our study provides evidence that the formation of pancreatic islet-like 3D structure can be significantly increased using gradient nanopattern chips, many polyhormonal cells were seen in the clusters, suggesting that the cluster were still immature and showed the phenotype of fetal pancreatic islet [39]. Thus further investigation focusing on biophysical and biochemical cues that regulates cellular maturation will be required to obtain functional pancreatic islets from hPSCs.

5. Conclusions

In summary, we have developed gradient-nanopatterned chips to screen various surface nanostructures efficiently and identified that a specific range of 200–300 nm nanopores (Po-2) favors pancreatic islet cluster differentiation in the presence of widely known soluble inducers. The clusters differentiated on the Po-2 pattern were able to further develop into pancreatic islet-like clusters with average size of 50 um, which would be an optimal size for cell transplantation. This result shows that providing optimal nanotopographical cues at specific differentiation steps can facilitate the production of homogeneously-sized clusters consisting of highly pure pancreatic endocrine cells. Thus, we suggest the gradient-nanopatterned chip provides a powerful tool to identify optimal nanostructures for specific cell types, which leads to efficient production of desired cells for cell therapies.

Acknowledgements

This research was supported by the Bio & Medical Technology Development Program of the National Research Foundation (NRF) funded by the Korean government (Ministry of Science & ICT) (No. 2017M3A9B4042581, 2018M3A9H1019504, 2017M3A9C6029563 and 2018R1C1B6002586).

Appendix A. Supplementary data

Supplementary data to this article can be found online at https://doi.org/10.1016/j.actbio.2018.12.011.

References

[1] D.H. Kim, P.P. Provenzano, C.L. Smith, A. Levchenko, Matrix nanotopography as a regulator of cell function, J. Cell Biol. 197 (3) (2012) 351–360.
[2] V. Ruprecht, P. Monzo, A. Ravasio, Z. Yue, E. Makhija, P.O. Strale, N. Gauthier, G. V. Shivashankar, V. Studer, C. Albiges-Rizo, V. Viasnoff, How cells respond to environmental cues - insights from bio-functionalized substrates, J. Cell Sci. 130 (1) (2017) 51–61.
[3] C.J. Bettinger, R. Langer, J.T. Borenstein, Engineering substrate topography at the micro- and nanoscale to control cell function, Angew. Chem. Int. Ed. Engl. 48 (30) (2009) 5406–5415.
[4] Y. Yang, K. Wang, X. Gu, K.W. Leong, Biophysical regulation of cell behavior-cross talk between substrate stiffness and nanotopography, Engineering (Beijing) 3 (1) (2017) 36–54.
[5] A. Fabienna, L. Oliver, Biophysical Properties of the Basal Lamina: A Highly Selective Extracellular Matrix, 2016
[6] F. Gattazzo, A. Urciuolo, P. Bonaldo, Extracellular matrix: a dynamic microenvironment for stem cell niche, Biochim. Biophys. Acta 1840 (8) (2014) 2506–2519.
[7] D. Bae, S.H. Moon, B.G. Park, S.J. Park, T. Jung, J.S. Kim, K.B. Lee, H.M. Chung, Nanotopographical control for maintaining undifferentiated human embryonic stem cell colonies in feeder free conditions, Biomaterials 35 (3) (2014) 916–928.
[8] C.W. Chang, Y. Hwang, D. Brafman, T. Hagan, C. Phung, S. Varghese, Engineering cell-material interfaces for long-term expansion of human pluripotent stem cells, Biomaterials 34 (4) (2013) 912–921.
[9] W.J. Hadden, J.L. Young, A.W. Holle, M.L. McFetridge, D.Y. Kim, P. Wijesinghe, H. Taylor-Weiner, J.H. Wen, A.R. Lee, K. Bieback, B.N. Vo, D.D. Sampson, B.F. Kennedy, J.P. Spatz, A.J. Engler, Y.S. Choi, Stem cell migration and mechanotransduction on linear stiffness gradient hydrogels, Proc. Natl. Acad. Sci. U.S.A. 114 (22) (2017) 5647–5652.
[10] S. Oh, K.S. Brammer, Y.S. Li, D. Teng, A.J. Engler, S. Chien, S. Jin, Stem cell fate dictated solely by altered nanotube dimension, Proc. Natl. Acad. Sci. U.S.A. 106 (7) (2009) 2130–2135.
[11] B.K. Teo, S.T. Wong, C.K. Lim, T.Y. Kung, C.H. Yap, Y. Ramagopal, L.H. Romer, E.K. Yim, Nanotopography modulates mechanotransduction of stem cells and induces differentiation through focal adhesion kinase, ACS Nano 7 (6) (2013) 4785–4798.
[12] J.H. Kim, H.W. Kim, K.J. Cha, J. Han, Y.J. Jang, D.S. Kim, J.H. Kim, Nanotopography promotes pancreatic differentiation of human embryonic stem cells and induced pluripotent stem cells, ACS Nano 10 (3) (2016) 3342–3355.
[13] P. Formentin, U. Catalan, M. Alba, S. Fernandez-Castillejo, R. Sola, J. Pallares, L.F. Marsal, Effects of SiO2 micropillar arrays on endothelial cells' morphology, N. Biotechnol. 33 (6) (2016) 781–789.
[14] K.S. Park, K.J. Cha, I.B. Han, D.A. Shin, D.W. Cho, S.H. Lee, D.S. Kim, Mass-producible nano-featured polystyrene surfaces for regulating the differentiation of human adipose-derived stem cells, Macromol. Biosci. 12 (11) (2012) 1480–1489.
[15] J.H. Kim, J.M. Auerbach, J.A. Rodriguez-Gomez, I. Velasco, D. Gavin, N. Lumelsky, S.H. Lee, J. Nguyen, R. Sanchez-Pernaute, K. Bankiewicz, R. McKay, Dopamine neurons derived from embryonic stem cells function in an animal model of Parkinson's disease, Nature 418 (6893) (2002) 50–56.
[16] J.H. Shim, J. Kim, J. Han, S.Y. An, Y.J. Jang, J. Son, D.H. Woo, S.K. Kim, J.H. Kim, Pancreatic islet-like three-dimensional aggregates derived from human embryonic stem cells ameliorate hyperglycemia in streptozotocin-induced diabetic mice, Cell Transplant. 24 (10) (2015) 2155–2168.
[17] J.H. Kim, M. Wang, J. Lee, H.J. Park, C. Han, H.S. Hong, J.S. Kim, G.H. An, K. Park, H.K. Park, S.F. Zhu, X.B. Sun, J.H. Kim, D.H. Woo, Prediction of hepatotoxicity for drugs using human pluripotent stem cell-derived hepatocytes, Cell Biol. Toxicol. 34 (1) (2018) 51–64.
[18] H.A. Russ, A.V. Parent, J.J. Ringler, T.G. Hennings, G.G. Nair, M. Shveygert, T. Guo, S. Puri, L. Haataja, V. Cirulli, R. Blelloch, G.L. Szot, P. Arvan, M. Hebrok, Controlled induction of human pancreatic progenitors produces functional beta-like cells in vitro, EMBO J. 34 (13) (2015) 1759–1772.
[19] T.C. Schulz, H.Y. Young, A.D. Agulnick, M.J. Babin, E.E. Baetge, A.G. Bang, A. Bhoumik, I. Cepa, R.M. Cesario, C. Haakmeester, K. Kadoya, J.R. Kelly, J. Kerr, L. A. Martinson, A.B. McLean, M.A. Moorman, J.K. Payne, M. Richardson, K.G. Ross, E.S. Sherrer, X. Song, A.Z. Wilson, E.P. Brandon, C.E. Green, E.J. Kroon, O.G. Kelly, K.A. D'Amour, A.J. Robins, A scalable system for production of functional pancreatic progenitors from human embryonic stem cells, PLoS One 7 (5) (2012) e37004.
[20] H. Takeuchi, N. Nakatsuji, H. Suemori, Endodermal differentiation of human pluripotent stem cells to insulin-producing cells in 3D culture, Sci. Rep. 4 (2014) 4488.
[21] B. Bose, P.S. Sudheer, In Vitro Differentiation of Pluripotent Stem Cells into Functional beta Islets Under 2D and 3D Culture Conditions and In Vivo Preclinical Validation of 3D Islets, Methods Mol. Biol. 1341 (2016) 257–284.
[22] J.A. Santiago, R. Pogemiller, B.M. Ogle, Heterogeneous differentiation of human mesenchymal stem cells in response to extended culture in extracellular matrices, Tissue Eng. Part A 15 (12) (2009) 3911–3922.
[23] A.B. McLean, K.A. D'Amour, K.L. Jones, M. Krishnamoorthy, M.J. Kulik, D.M. Reynolds, A.M. Sheppard, H. Liu, Y. Xu, E.E. Baetge, S. Dalton, Activin a efficiently specifies definitive endoderm from human embryonic stem cells

only when phosphatidylinositol 3-kinase signaling is suppressed, Stem Cells 25 (1) (2007) 29–38.
[24] P. Gadue, T.L. Huber, P.J. Paddison, G.M. Keller, Wnt and TGF-beta signaling are required for the induction of an in vitro model of primitive streak formation using embryonic stem cells, Proc. Natl. Acad. Sci. U.S.A. 103 (45) (2006) 16806–16811.
[25] M. Johannesson, A. Stahlberg, J. Ameri, F.W. Sand, K. Norrman, H. Semb, FGF4 and retinoic acid direct differentiation of hESCs into PDX1-expressing foregut endoderm in a time- and concentration-dependent manner, PLoS One 4 (3) (2009) e4794.
[26] A.M. Zorn, J.M. Wells, Vertebrate endoderm development and organ formation, Annu. Rev. Cell Dev. Biol. 25 (2009) 221–251.
[27] A. Kubo, R. Stull, M. Takeuchi, K. Bonham, V. Gouon-Evans, M. Sho, M. Iwano, Y. Saito, G. Keller, R. Snodgrass, Pdx1 and Ngn3 overexpression enhances pancreatic differentiation of mouse ES cell-derived endoderm population, PLoS One 6 (9) (2011) e24058.
[28] R. Desgraz, P.L. Herrera, Pancreatic neurogenin 3-expressing cells are unipotent islet precursors, Development 136 (21) (2009) 3567–3574.
[29] K.A. D'Amour, A.G. Bang, S. Eliazer, O.G. Kelly, A.D. Agulnick, N.G. Smart, M.A. Moorman, E. Kroon, M.K. Carpenter, E.E. Baetge, Production of pancreatic hormone-expressing endocrine cells from human embryonic stem cells, Nat. Biotechnol. 24 (11) (2006) 1392–1401.
[30] O.G. Kelly, M.Y. Chan, L.A. Martinson, K. Kadoya, T.M. Ostertag, K.G. Ross, M. Richardson, M.K. Carpenter, K.A. D'Amour, E. Kroon, M. Moorman, E.E. Baetge, A.G. Bang, Cell-surface markers for the isolation of pancreatic cell types derived from human embryonic stem cells, Nat. Biotechnol. 29 (8) (2011) 750–756.
[31] M.J. Doyle, L. Sussel, Nkx2.2 regulates beta-cell function in the mature islet, Diabetes 56 (8) (2007) 1999–2007.
[32] T. Toyoda, S. Mae, H. Tanaka, Y. Kondo, M. Funato, Y. Hosokawa, T. Sudo, Y. Kawaguchi, K. Osafune, Cell aggregation optimizes the differentiation of human ESCs and iPSCs into pancreatic bud-like progenitor cells, Stem Cell Res. 14 (2) (2015) 185–197.
[33] K. Tateishi, J. He, O. Taranova, G. Liang, A.C. D'Alessio, Y. Zhang, Generation of insulin-secreting islet-like clusters from human skin fibroblasts, J. Biol. Chem. 283 (46) (2008) 31601–31607.
[34] M. Takeichi, The cadherins: cell-cell adhesion molecules controlling animal morphogenesis, Development. 102 (4) (1988) 639–655.
[35] S.J. Kim, Y.S. Choi, S.M. Kim, S.M. Lim, H.S. Jun, E.Y. Park, O.K. Hwang, C.W. Lee, D.I. Kim, Pancreatic islet-like clusters from periosteum-derived progenitor cells, Biotechnol. Bioproc. E. 18 (6) (2013) 1116–1121.
[36] J. Jeon, M. Correa-Medina, C. Ricordi, H. Edlund, J.A. Diez, Endocrine cell clustering during human pancreas development, J. Histochem. Cytochem. 57 (9) (2009) 811–824.
[37] A. Kim, K. Miller, J. Jo, G. Kilimnik, P. Wojcik, M. Hara, Islet architecture: A comparative study, Islets 1 (2) (2009) 129–136.
[38] R. Lehmann, R.A. Zuellig, P. Kugelmeier, P.B. Baenninger, W. Moritz, A. Perren, P.A. Clavien, M. Weber, G.A. Spinas, Superiority of small islets in human islet transplantation, Diabetes 56 (3) (2007) 594–603.
[39] M.J. Riedel, A. Asadi, R. Wang, Z. Ao, G.L. Warnock, T.J. Kieffer, Immunohistochemical characterisation of cells co-producing insulin and glucagon in the developing human pancreas, Diabetologia 55 (2) (2012) 372–381.